Solid State Sciences 61 (2016) 155–160

Contents lists available at ScienceDirect

Solid State Sciences

journal homepage: www.elsevier.com/locate/ssscie

The structure and phase transitions in oxyfluoride $(ND_4)_2MoO_2F_4$

Evgeniy V. Bogdanov [a, b], Svetlana V. Mel'nikova [a], Evgeniy I. Pogoreltsev [a, c, *], Maxim S. Molokeev [a, d], Igor N. Flerov [a, c]

[a] Kirensky Institute of Physics, Siberian Branch of RAS, 660036 Krasnoyarsk, Russia
[b] Krasnoyarsk State Agrarian University, 660049 Krasnoyarsk, Russia
[c] Institute of Engineering Physics and Radioelectronics, Siberian State University, 660074 Krasnoyarsk, Russia
[d] Far Eastern State Transport University, 680021 Khabarovsk, Russia

ARTICLE INFO

Article history:
Received 24 May 2016
Received in revised form
17 August 2016
Accepted 20 August 2016
Available online 22 August 2016

ABSTRACT

Single crystals of $(ND_4)_2MoO_2F_4$ containing 95% deuterium were produced by repeated recrystallization of $(NH_4)_2MoO_2F_4$ in heavy water. The effect of deuteration on the parameters of successive phase transitions was investigated by differential scanning microcalorimetry and polarization optics. X-ray analysis of the original and distorted phases was performed. It was found that deuteration does not change the sequence of crystal phases typical for $(NH_4)_2MoO_2F_4$, but leads to a shift in the phase transition *Cmcm* → *Pnma* towards the tricritical point. The mechanism of phase transitions in $(ND_4)_2MoO_2F_4$ was associated with both the ordering and the displacement of atoms.

1. Introduction

Oxygen-fluorine compounds are interesting because of the possibility of obtaining piezoelectric, pyroelectric and ferroelectric properties at room temperature in these crystals, caused by the acentric quasioctahedron anionic group MeO_xF_{6-x} [1]. In addition, one of the rapidly developing areas in this research field is related to the search for possible disorder in the original structure of orthorhombic oxyfluorides and the establishment of conditions for the loss of stability as a result of order-disorder phase transitions [2–6]. As a rule, the barocaloric effect appears at such significant structural transformations, allowing us to consider these materials as promising solid-state refrigerants [6,7].

Complex investigations have shown that, irrespective of the cationic composition, the compounds $A^+{}_2Me^{6+}O_2F_4$ (A: K, Rb, NH4; Me: W, Mo) are characterized by orthorhombic symmetry at room temperature, with the *Cmcm* space group ($Z = 4$) [4,5], and experiencing two successive phase transitions: $G_0(T_1) \rightarrow G_1(T_2) \rightarrow G_2$. In spite of the slight difference in the ionic radii of W (0.60 Å) and Mo (0.59 Å) atoms, replacement of the central atom leads to a significant increase in the T_1 and T_2 temperatures, leading to the expansion of the temperature range of stability of the G_1 phase and an anomalously large value of the baric coefficient dT_1/dp for $(NH_4)_2MoO_2F_4$ [2,3]. It is possible that these features are caused by the different nature of structural transformations at T_1; in the tungsten compound, this is a transition to the ferroelastic phase, while in the molybdenum compound, this is antiferroelectric.

A significant amount of the entropy change $\Delta S_1/R \gg \ln 2$ for ammonium oxyfluorides $A^+{}_2Me^{6+}O_2F_4$ clearly shows the leading role of ordering processes in the mechanism of structural distortion at T_1. The cationic substitution Rb → NH_4 causes a change in the order of the phase transition from the first to the second, and a significant decrease in entropy. However, the value of ΔS_1 remains characteristic for the order-disorder transformation ($\Delta S_1/R \approx 3$) in $Rb_2MoO_2F_4$. The most interesting aspect is the gradual substitution of ammonium for rubidium in a solid solution system, $(NH_4)_{2-x}Rb_xMoO_2F_4$ [8]. The antiferroelectric state below T_1 remains up to $x = 1.8$. With higher concentrations of Rb, there is a transition to the ferroelastic phase *P*-1, as observed in $(NH_4)_2WO_2F_4$.

Partial or full ordering of the O and F ligands due to the formation of hydrogen bonds at T_1 is observed when Rb is substituted with NH_4, which changes the polarizability of ammonium, and in turn leads to stronger physical properties in ammonium crystals than in $Rb_2MoO_2F_4$. Decreasing the $\Delta S_1/R$ value in $Rb_2MoO_2F_4$ compared with $(NH_4)_2MoO_2F_4$ shows the direct participation of NH_4 cations in the $G_0 \rightarrow G_1$ transition and an indirect impact (through octahedral anions) to the $G_1 \rightarrow G_2$ transition [9].

The phase transition at T_2 in $A^+{}_2Me^{6+}O_2F_4$ proceeds as a second order transformation, regardless of the size of the cations A^+ and

* Corresponding author. Kirensky Institute of Physics, Siberian Branch of RAS, 660036 Krasnoyarsk, Russia.
E-mail address: pepel@iph.krasn.ru (E.I. Pogoreltsev).

http://dx.doi.org/10.1016/j.solidstatesciences.2016.08.012
1293-2558/

Me^{6+}. The proximity of entropy values $\Delta S_2/R$ suggests that the mechanism of the $G_1 \rightarrow G_2$ transition is the same in different compounds, namely the displacement type, and is not associated with the presence or absence of an ammonium cation NH_4 in the structure [8].

On the one hand, deuteration has little effect on the transition temperature observed in ferroelastic $(NH_4)_2WO_2F_4$, indicating the absence of hydrogen bonds N–H···F(O) in the initial phase (sp. gr. *Cmcm*). On the other hand, it leads to a significant increase in dT_2/dp and thus a pinching out G_1 phase and a significant decrease in $\Delta S_1/R$ entropy [10].

In this paper, in order to clarify the role of ammonium groups in the mechanism and the nature of phase transitions in antiferroelectric oxyfluoride $(NH_4)_2MoO_2F_4$, synthesis, searching for phase transitions by optical and calorimetric methods and studies on the structure of the deuterated crystal $(ND_4)_2MoO_2F_4$ were performed.

2. Synthesis of the samples

Synthesis of the deuterated compound $(ND_4)_2MoO_2F_4$ occurred in three stages. At the first stage, $(NH_4)_2MoO_4$ was prepared by heating an NH_4OH-solution (~100 ml) while slowly mixing in molybdenum oxide (~20 g). Precipitation of the compound $(NH_4)_2MoO_4$ was followed by the gradual addition of 100 ml of C_2H_5OH to the solution.

At the second stage, $(NH_4)_3MoO_3F_3$ received by adding $3HF + 2NH_4OH + 2HF$ to the starting compound $(NH_4)_2MoO_4$. The resulting complex, $(NH_4)_3MoO_3F_3$, dissolved in hydrofluoric acid to form protonated $(NH_4)_2MoO_2F_4$:

$$(NH_4)_3MoO_3F_3 + HF = (NH_4)_2MoO_2F_4\ NH_3 + H_2O$$

At the third stage, $(NH_4)_2MoO_2F_4$ (~4 g) was dissolved in heavy water (99.9% D). The solution was placed in a desiccator with phosphorus oxide P_2O_5 and was kept there until complete absorption of the water had occurred. Next, the compound $(ND_4)_2MoO_2F_4$ was recrystallized several times in heavy water to obtain the maximum possible degree of deuteration. As a result, small single crystals of $(ND_4)_2MoO_2F_4$ were obtained, with a deuteration ratio of 95% determined by comparing the integral of the absorption lines (NMR ^1H) of the proton and deuterated compounds.

Our preliminary X-ray studies showed that the $(ND_4)_2MoO_2F_4$ crystals had orthorhombic symmetry (sp. gr. *Cmcm*) at room temperature.

3. Initial studies

To obtain information about the presence of phase transitions, their temperatures, the heat capacity and integrated energy parameters, the synthesized compound $(ND_4)_2MoO_2F_4$ was studied by differential scanning microcalorimetry (DSM) and with a polarizing microscope.

The main calorimetric experiments were performed in a wide temperature range of 100–400 K in a helium atmosphere at a rate of $dT/d\tau = 8$ K/min upon heating and cooling. Heat capacity measurements were made on several samples with mass of about 0.2 g. Two reproducible anomalies were found on a temperature dependence of the specific heat $C_p(T)$ during thermal cycling.

Fig. 1 shows the temperature dependence of the excess heat capacity ΔC_p, associated with phase transitions. ΔC_p is the difference between the total molar heat capacity C_p and the non-anomalous lattice contribution C_{latt}. The peaks of ΔC_p correspond to phase transition temperatures $T_1 = 275 \pm 1$ K, and $T_2 = 201 \pm 5$ K in heating mode. High-temperature transformation indicated the

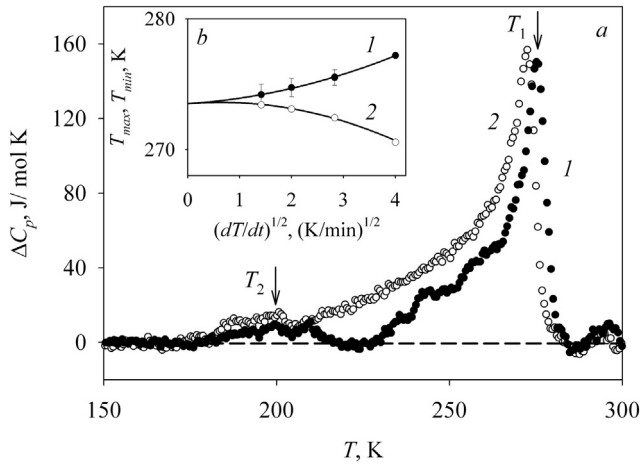

Fig. 1. Anomalous heat capacity of the crystal $(ND_4)_2MoO_2F_4$, measured by DSM in the heating (1) and cooling (2) modes at a temperature rate $dT/d\tau = 8$ K/min (*a*). Dependence of the T_1 phase transition temperature of a heating (1) and cooling (2) rate (*b*).

first order phase transition with a temperature hysteresis $\delta T_1 = 3$ K at a rate of temperature cycling equal to 8 K/min. To determine the real hysteresis corresponding to quasi-static conditions, the temperature T_1 was determined depending on the rate of heating and cooling, which was varied over a wide range of $dT/d\tau = \pm$ (2–16) K/min (Fig. 1b). Extrapolation of the experimental dependence $T_i(dT/d\tau)^{1/2}$ to quasi-equilibrium conditions ($dT/d\tau = 0$) leads to the following parameters: $T_1 = 273.5 \pm 1$ K and $\delta T_1 \geq 0$. Temperature hysteresis defined this way showed that the high temperature transition was the first order transformation very close to the tricritical point.

The enthalpy changes ΔH_i associated with phase transitions were determined by integration of the $\Delta C_p(T)$ functions. The corresponding values were strongly different: $\Delta H_1 = 2500 \pm 250$ J/mol and $\Delta H_2 = 200 \pm 20$ J/mol, which indicates different types of structural transformations.

In the next stage of the study, the stability of the initial phase (sp. gr. *Cmcm*) was assessed by measuring the temperature dependence of birefringence $\Delta n(T)$ using a Berek compensator (Leica) on an *Axioskop 40* polarizing microscope with a *Linkam LTS – 350* thermal camera. The samples of $(ND_4)_2MoO_2F_4$ were selected as single crystal plates (010) with a thickness of $h = 70 \pm 1$ μm. This choice of orientation of the samples was made since the crystals grow with a good face (010); this provides the opportunity to use the growth plate. The possible error in determining the absolute value of birefringence was ±0.0002.

The results of the birefringence temperature dependence of $(ND_4)_2MoO_2F_4$ crystals in conjunction with the protonated compound obtained previously are shown in Fig. 2*a* [11]. One can see that, at high temperatures, $\Delta n_b(T)$ was linear for both compounds. Birefringence in the deuterated sample varied continuously, almost without any jump in $\Delta n_b(T)$, which was very different from the birefringence in the protonated compound, in which there was an abrupt change in birefringence at temperatures $T_{1\downarrow} = 267.2$ K and $T_{1\uparrow} = 267.8$ K and a rather large temperature hysteresis $\delta T_1 \approx 0.6$ K. This shows that the phase transition at $T_1 = 275$ K in $(ND_4)_2MoO_2F_4$ crystal acquires the features of the second order transformation. A further decrease in temperature leads to a gradual rise in optical anisotropy and to saturation of $\Delta n_b(T)$ close to $T_2 = 180$ K.

The temperature dependence of birefringence was linearly extrapolated from the initial phase to the low-temperature area in order to determine the anomalous part of birefringence $\delta n_b(T)$,

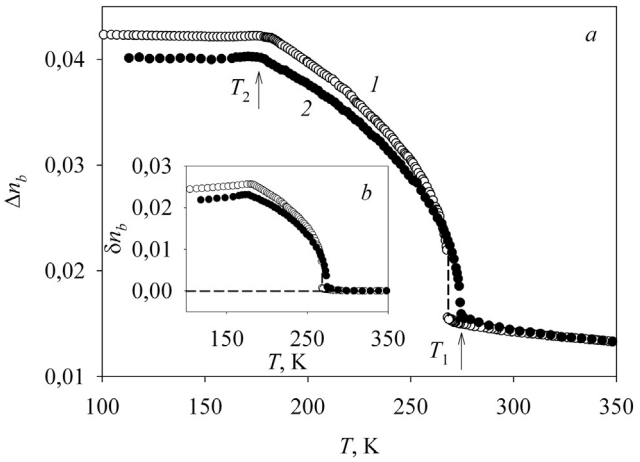

Fig. 2. The temperature dependence of the birefringence $\Delta n_b(T)$ for both $(NH_4)_2MoO_2F_4$ (*1*) and $(ND_4)_2MoO_2F_4$ (2) (*a*). The temperature behavior of the anomalous contribution of $\delta n_b(T)$ (*b*).

which is a deviation of $\Delta n_b(T)$ from the starting dependence at the phase transition (Fig. 2b). Strong changes in the refractive indices of both crystals were observed below T_1. However, substitution of the ammonium group $(ND_4) \rightarrow (NH_4)$ led to a ~10% decrease in anomalous birefringence $\delta n_b(T)$ in $(ND_4)_2MoO_2F_4$.

According to a previous study [5], there is a partial ordering of fluorine and oxygen ligands and complete ordering of ammonium groups with the formation of hydrogen bonds N–H···F(O) at T_1 in $(NH_4)_2MoO_2F_4$ crystals. The polarizability of ammonium ions varies due to the latter circumstance, which leads to strong anomalies in birefringence. D → H substitution leads to a decrease in $\delta n_b(T)$ in $(ND_4)_2MoO_2F_4$ due to the increased connection N–D···F(O) and reduced electronic polarizability of the (ND_4) tetrahedral cation.

4. X-ray diffraction analysis

The data collection for the $(ND_4)_2MoO_2F_4$ single crystal was performed using a *Bruker SMART APEX II* (*Bruker AXS*) diffractometer with graphite-monochromated Mo-Kα radiation (λ = 0.71073 Å) using the ω–2θ scan technique. Typical sample handling methods and measurement conditions can be found elsewhere [12].

All reflections were indexed to the orthorhombic unit cell (sp.gr. *Cmcm*) with parameters close to the cell parameters of $(NH_4)_2MoO_2F_4$ [5] and $(ND_4)_2WO_2F_4$ [4]. The absorption corrections were applied using the *SADABS* program. The structure was solved by direct methods using the *SHELXS* package and refined in the anisotropic approach for non-hydrogen atoms using the *SHELXL* program. During refinement, the Mo^{6+} ion was disordered over four 16*h* Wyckoff positions. Owing to this, low values of *R*-factors and a stable refinement process were achieved (Table 1). The coordinates of the atoms and the thermal parameters are provided in Table 2. One can see that the initial phase (sp.gr. *Cmcm*) contains one O^{2-} and one F^- ion which occupy one site with different occupancy.

Thermal investigations into the structure of $(ND_4)_2MoO_2F_4$ were performed using a *D8 ADVANCE* (*Bruker*) powder diffractometer equipped with a *VANTEC* detector with an Ni filter and *TTK*-450 (*ANTON PAAR*) thermal attachment. The measurements were made using Cu-Kα radiation. The powder diffraction method was used since single crystal destruction at the phase transition led to several domains which prevented good single crystal measurements. A detailed description of the experimental set up can be found elsewhere [13–15].

Three powder patterns with high exposure time were measured at $T = 303$, 233 and 133 K, and 18 additional patterns were collected in the temperature range of 303–133 K with a 10 K step and lower exposure time (Fig. 3) in order to plot the dependence of cell parameters on temperature.

The Rietveld refinement was performed by the *TOPAS* 4.2 program [16]. Almost all peaks of the initial phase G_0 at $T = 303$ K were indexed by the orthorhombic unit cell (sp.gr. *Cmcm*). Small unindexed peaks corresponding to small amounts of the impurity $(NH_4)_2MoO_3F_2$ (~5.2(2)%), confirmed the relatively high degree of purity of the deuterated compound. The refinement process was stable and led to low *R*-factors (Table 3, Fig. 4). Main bond lengths are in Table 4.

Low-temperature experiments performed in a wide temperature range (Fig. 3) showed the appearance of superstructure peaks at $T_1 = 270$ K, which are forbidden for the space group *Cmcm* of the G_0 phase. All these additional peaks can be described by the emergence of instability at (1, 0, 0) *k*15 – point (*Y*) of the Brillouin zone of the G_0 - *Cmcm* unit cell. Moreover, there were no main peaks with splitting or broadening (Fig. 3), which indicates that the symmetry of the distorted unit cell remained orthorhombic.

Analysis of the possible structural distortions associated with the phase transition at T_1 using the *ISODISTORT* program [17] allowed us to choose a unit cell with new cell parameters: $a' = c$, $b' = a$; $c' = b$, with the origin shift on (1/4, 1/4, 0). Here, the *a'*, *b'*, *c'* is the basis of the new distorted unit cell of the G_1 phase; *a*, *b*, *c* is the basis of the initial phase G_0 (sp.gr. *Cmcm*). *ISODISTORT* suggested seven probable space groups: *Pmma*, *Pnna*, *Pbcm*, *Pnnm*, *Pmmn*, *Pbcn* and *Pnma*, which can account for the superstructure peaks. However, only *Pmma* and *Pnma* allowed us to index all

Table 2
Coordinates of atoms, equivalent thermal parameters U_{eq} and occupancies p of G_0 phase (*Cmcm*), obtained from single crystal experiment.

Atom	Wyck.	*x*	*y*	*z*	B_{iso}	p
Mo	4*c*	0.0150 (4)	0.10600 (4)	0.2334 (2)	2.40(3)	1/4
F1	16*h*	0.2268 (4)	0.11920 (18)	0.4351 (3)	3.69(5)	3/4
O1	16*h*	0.2268 (4)	0.11920 (18)	0.4351 (3)	3.69(5)	1/4
O2	4*c*	1/2	0.4878 (3)	1/4	3.37(9)	1
F2	4*c*	1/2	0.2542 (3)	3/4	4.8(1)	1
N1	4*c*	1/2	−0.0608 (5)	1/4	3.3(1)	1
N2	4*c*	1/2	0.2707 (5)	1/4	3.4(1)	1

Table 1
Main parameters of single crystal experiment and crystal structure refinement of $(ND_4)_2MoO_2F_4$ in G_0 phase.

Space group, *Z*	*Cmcm*, 4	Temperature (K)	296
a (Å)	5.9630(8)	Crystal size (mm)	0.2 × 0.2 × 0.1
b (Å)	14.4743(18)	$2\theta_{max}$ (°)	29.62
c (Å)	7.1100(9)	R_{int}	0.0259
V (Å^3)	613.67(14)	*R*1/*wR*2 [$F_o > 4\sigma(F_o)$]	0.0334/0.0963
$\rho_{выч}$ (г/см^3)	2.511	*Goof*	1.020
M_r	231.96	$\Delta\rho_{max}/\Delta\rho_{min}$ (e/Å^3)	0.868/−0.931
Measured reflections/Independent reflections/refined parameters	2957/498/33	*h*, *k*, *l* - limits	$-8 \le h \le 8$; $-19 \le k \le 19$; $-9 \le l \le 9$

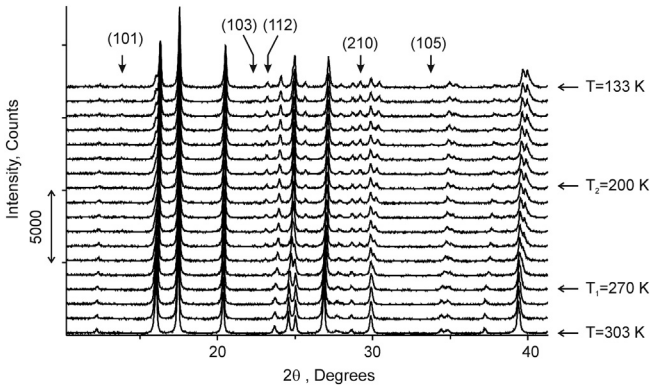

Fig. 3. Powder patterns of $(ND_4)_2MoO_2F_4$ in the temperature range of 303–133 K. Arrows show superstructure peaks appeared at $T < 270$ K.

refine the crystal structure of the G_1 phase.

The crystal structure model of the G_1 phase was generated using the G_0 phase, the *ISODISTORT* program and a critical irreducible representation and order parameter $Y_2^-(\eta)$ of the phase transition *Cmcm* → *Pnma*. The crystal structure refinement in the *TOPAS* 4.2 program was stable and led to low *R*-factors (Table 3, Fig. 5). The coordinates of the atoms of the G_1 phase are shown in Table 5. Assignment of O and F ions were checked using bond lengths (Table 4). For example, big bond lengths d(Mo–F3) = 1.942(7) Å and d(Mo–F2) = 2.004(5) Å mean that F3 and F2 are actually fluorine ions, otherwise short d(Mo–O2) and average d(Mo–F1/O1) lengths (Table 4) mean that O2 is oxygen ion and F1/O1 is a mix of F/O ions.

There were no additional superstructure peaks or main peak splitting/broadening at $T_2 = 200$ K. Therefore, symmetry, orientation of the axis and cell parameters should not change at this phase transition. However, the thermal dependence of cell parameters and cell volume showed a fracture at T_2, which corresponds to a phase transition (Fig. 6) observed by calorimetric and optical experiments. Therefore, the spacegroup should be changed at T_2. The irreducible representation *GM* associated with $k = (0,0,0)$ in the Brillouin zone of the G_0 phase drives this phase transition. Theoretical group analysis performed by the *ISODISTORT* program revealed 17 possible space groups, of which only four, i.e. *Pnma*, $P2_12_12_1$, $Pmc2_1$ and $Pna2_1$, indexed all superstructure peaks in the powder pattern and did not generate unobserved peaks. Further reduction of the list of possible space groups was done after obtaining strong evidence about the existence or absence of the center of inversion in the G_2 phase. These experiments are planned in further.

Table 3
Main parameters of powder diffraction experiment and crystal structure refinement of $(ND_4)_2MoO_2F_4$ in G_0, G_1 phases. Possible space groups of G_2 phase and cell parameters.

Phase	G_0	G_1	G_2
Temperature, K	303	233	133
Space group	*Cmcm*	*Pnma*	*Pnma*, $P2_12_12_1$, $Pmc2_1$ or $Pna2_1$
a, Å	5.96051(12)	7.1258(2)	7.14843(16)
b, Å	14.4679(2)	5.91490(13)	5.86197(13)
c, Å	7.10667(15)	14.3030(3)	14.2285(3)
V, Å^3	612.85(2)	603.69(2)	596.23(2)
2θ interval, °	5–120	5–120	5–120
$R_{wp}/R_p/R_B$, %	6.80/5.00/2.12	6.94/5.29/2.31	–
χ^2	2.088	2.134	–

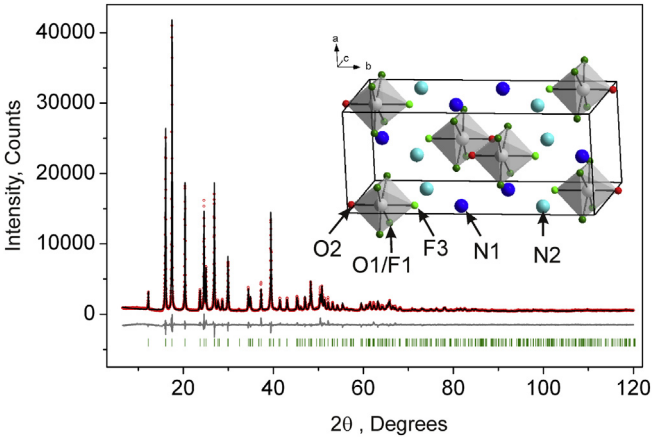

Fig. 4. Difference Rietveld plot of G_0 phase of $(ND_4)_2MoO_2F_4$. Inset shows crystal structure.

Table 4
Main bond lengths d(Mo–O/F) in G_0, G_1 phases.

G_0		G_1	
Bond	Length, Å	Bond	Length, Å
(Mo–O2) × 1	1.731(6)	(Mo–O2) × 1	1.706(8)
(Mo–F1/O1) × 4	1.889(3)	(Mo–F1/O1) × 2	1.745(6)
(Mo–F3) × 1	1.978(6)	(Mo–F3) × 1	1.942(7)
		(Mo–F2) × 2	2.004(5)

experimentally observed superstructure peaks. Regarding that of symmetry, that of *Pnma* is higher than *Pmma*, so *Pnma* was used to

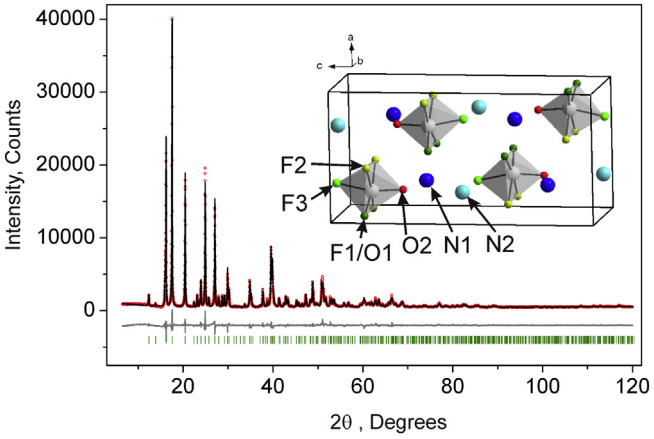

Fig. 5. Difference Rietveld plot of G_1 phase of $(ND_4)_2MoO_2F_4$. Inset shows crystal structure.

Table 5
Coordinates of atoms, isotropic thermal parameters B_{iso} and occupations p of G_1 phase (*Pnma*), obtained from Rietveld refinement.

Atom	Wyck.	x	y	z	B_{iso}	p
Mo	4*c*	0.71203 (18)	0.25	0.63949 (10)	2.85 (13)	1
F1	8*d*	0.5512 (8)	0.0300 (9)	0.6267 (3)	1.04 (17)	1/2
O1	8*d*	0.5512 (8)	0.0300 (9)	0.6267 (3)	1.04 (17)	1/2
F2	8*d*	−0.0830 (7)	0.0183 (7)	0.6379 (3)	1.33 (16)	1
F3	4*c*	0.7694 (12)	0.25	0.5068 (5)	3.8 (2)	1
O2	4*c*	0.7254 (15)	0.25	0.7586 (5)	3.0 (3)	1
N1	4*c*	0.2719 (14)	0.25	0.1899 (4)	2.1 (3)	1
N2	4*c*	0.2099 (19)	0.25	0.5152 (8)	7.1 (5)	1

(Fig. 2).

From a comparison of Tables 2 and 5 as well as Figs. 4 and 5, it is evident that the main processes at the $G_0 \rightarrow G_1$ phase transition are complete ordering of the Mo central atom and partial ordering of F1/O1 ions. These two processes are related due to the fact that the movement of the central atom is caused by the need to ensure the shortest Mo–O distance. However, slight displacement of the ions takes place in addition to ordering.

Only complete ordering of the central atom should be accompanied by an R ln 4 entropy change. However, the experimentally measured entropy of the $G_0 \rightarrow G_1$ phase transition obtained from

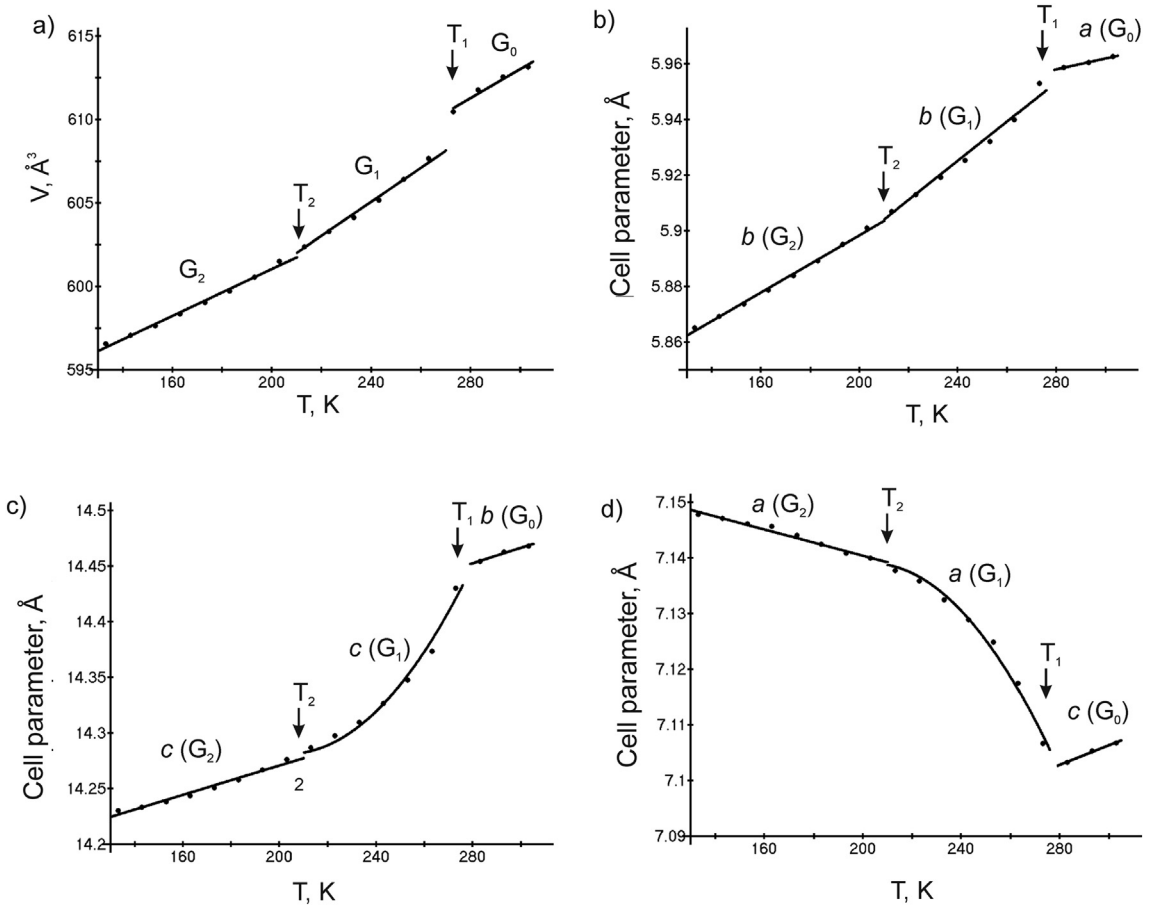

Fig. 6. Temperature dependence of cell volume (*a*) and cell parameters (*b*, *c*, *d*) of different phases.

5. Discussion of the results

The high degree of deuteration did not effect on the sequence of crystalline phase changes, which were observed in the initial compound $(NH_4)_2MoO_2F_4$ [5]. However, there was a decrease in the unit cell volume of the initial phase (~0.2%), which showed an increase in the chemical pressure, and according to the phase $T-p$ diagram of $(NH_4)_2MoO_2F_4$, which should lead to an increase in the phase transition temperatures in $(ND_4)_2MoO_2F_4$ [3,6]. This effect was reliably observed for the $G_0 \rightarrow G_1$ phase transition; in accordance with the DSM data and optical measurements, there was an increase in T_1 up to ~5–8 K. In addition, D → H substitution caused the displacement of the structural transformation towards the tricritical point, as evidenced by the lack of both δT_1 hysteresis and $\delta n_b(T)$ jump in $(ND_4)_2MoO_2F_4$ compared to $(NH_4)_2MoO_2F_4$ [11] DSM appeared to be less that $\Delta S_1 \approx 9.2$ J/mol K ≈ 1.1 R $\approx$ R ln 3. Regarding the DSM method, on the one hand, it is characterized by low sensitivity to relatively small changes in the anomalous heat capacity over a wide temperature range but, on the other hand, it does not reveal the contribution of latent heat. It is expected that the actual change in the entropy value at T_1 was higher. This situation has been observed many times, particularly in the study of $(ND_4)_2WO_2F_4$ [10].

Based on the temperature dependence of the lattice parameters, it can be seen that the phase transition at T_2 is a structural transformation that is accompanied by a slight change in the unit cell volume. All the atoms in the unit cell are displaced in different directions as a result of this transition. Unfortunately, since the compound $(ND_4)_2MoO_2F_4$ could not be obtained as a bulk single crystal to perform searching for second harmonic generation, the

question about the presence of an inversion center in the G_2 phase is still open. Therefore, it is difficult to consider the particular model of atomic displacements at T_2.

Calorimetric, X-ray and optical data analysis demonstrated the strong possibility of saving the antiferroelectric state in the distorted G_1 phase of $(ND_4)_2MoO_2F_4$, which was energetically more favorable, as particularly shown in the study of solid solutions $(NH_4)_2W_{1-x}Mo_xO_2F_4$ [18]. The ferroelectric polar state in the distorted low temperature G_2 phase was also not excluded.

6. Conclusion

The highlights of the deuteration effect on $(NH_4)_2MoO_2F_4$ are as follows:

1. A molybdenum oxyfluoride appeared to be more susceptible to the replacement of protons by deuterons in comparison with a related tungsten oxyfluoride, as evidenced by a higher degree of deuteration (95% versus 85%) for the same number of recrystallizations in heavy water.
2. The D → H substitution did not lead to significant changes in the stability ranges of the initial and distorted phases, but caused a marked approximation of the phase transition at T_1 to the tricritical point.
3. The mechanism of phase transitions in $(ND_4)_2MoO_2F_4$ were associated with both ordering processes and displacement of the central atom as well as partial ordering of some F/O atoms.

Acknowledgments

The authors are grateful to A.G. Kocharova for the synthesis and deuteration of the samples, and to A.A. Sukhovsky and Y.N. Ivanov for the execution of NMR studies to determine the degree of sample deuteration.

This study was partially supported by Russian Foundation for Basic Research, project No. 16–32–00201 mol_a.

References

[1] K.R. Heier, A.J. Norquist, P.S. Halasyamani, A. Duarte, C.L. Stern, K.R. Poeppelmeier, Inorg. Chem. 38 (1999) 762.
[2] I.N. Flerov, V.D. Fokina, M.V. Gorev, A.D. Vasiliev, A.F. Bovina, M.S. Molokeev, A.G. Kocharova, N.M. Laptash, Phys. Solid State 48 (4) (2006) 759–764.
[3] V.D. Fokina, E.V. Bogdanov, E.I. Pogorel'tsev, V.S. Bondarev, I.N. Flerov, N.M. Laptash, Phys. Solid State 52 (1) (2010) 158–166.
[4] A.A. Udovenko, N.M. Laptash, Acta Cryst. B64 (2008) 645.
[5] A.A. Udovenko, A.D. Vasiliev, N.M. Laptash, Acta Cryst. B66 (2010) 34.
[6] M.V. Gorev, E.V. Bogdanov, I.N. Flerov, A.G. Kocharova, N.M. Laptash, Phys. Solid State 52 (1) (2010) 167–175.
[7] G.Z. Pinksner, V.G. Kuznetsov, Kristallographia 13 (1) (1968) 74.
[8] E.V. Bogdanov, A.D. Vasil'ev, I.N. Flerov, N.M. Laptash, Phys. Solid State 53 (2) (2011) 303–308.
[9] S.V. Mel'nikova, N.M. Laptash, Phys. Solid State 57 (6) (2015) 1201–1205.
[10] I.N. Flerov, V.D. Fokina, M.V. Gorev, E.V. Bogdanov, M.S. Molokeev, A.F. Bovina, A.G. Kocharova, Phys. Solid State 49 (6) (2007) 1149–1156.
[11] S.V. Mel'nikova, N.M. Laptash, Phys. Solid State 50 (3) (2008) 511–514.
[12] V.V. Atuchin, L.I. Isaenko, V.G. Kesler, L. Kang, Z.S. Lin, M.S. Molokeev, A.P. Yelisseyev, S.A. Zhurkov, J. Phys. Chem. C 117 (2013) 7269–7278.
[13] V.V. Atuchin, M.S. Molokeev, G. Yu Yurkin, T.A. Gavrilova, V.G. Kesler, N.M. Laptash, I.N. Flerov, G.S. Patrin, J. Phys. Chem. C 116 (2012) 10162–10170.
[14] N.N. Golovnev, M.S. Molokeev, S.N. Vereshchagin, V.V. Atuchin, J. Coord. Chem. 66 (23) (2013) 4119–4130.
[15] V.V. Atuchin, A.S. Aleksandrovsky, O.D. Chimitova, T.A. Gavrilova, A.S. Krylov, M.S. Molokeev, A.S. Oreshonkov, B.G. Bazarov, J.G. Bazarova, J. Phys. Chem. C 118 (28) (2014) 15401–15411.
[16] Bruker AXS, TOPAS V4: User's Manual, Bruker AXS, Karlsruhe, Germany, 2008.
[17] B.J. Campbell, H.T. Stokes, D.E. Tanner, D.M. Hatch, J. Appl. Crystallogr. 39 (4) (2006) 607.
[18] E.V. Bogdanov, E.I. Pogoreltsev, S.V. Mel'nikova, M.V. Gorev, I.N. Flerov, M.S. Molokeev, A.V. Kartashev, A.G. Kocharova, N.M. Laptash, Phys. Solid State 55 (2) (2013) 409–418.